



Particle acoustic detection in gravitational wave aluminum resonant antennas

B. Buonomo ^a, E. Coccia ^{b,c,d}, S. D'Antonio ^b, G. Delle Monache ^a,
D. Di Gioacchino ^a, V. Fafone ^a, C. Ligi ^a, A. Marini ^{a,*}, G. Mazzitelli ^a,
G. Modestino ^a, S. Panella ^a, G. Pizzella ^{a,c}, L. Quintieri ^a, S. Roccella ^{a,1},
F. Ronga ^a, P. Tripodi ^a, P. Valente ^{a,2}

^a *Istituto Nazionale di Fisica Nucleare—Laboratori Nazionali di Frascati, Via E. Fermi, 40-00044 Frascati, Italy*

^b *Istituto Nazionale di Fisica Nucleare—Sezione Roma2, Via della Ricerca Scientifica, 1-00133 Rome, Italy*

^c *Dipartimento di Fisica, Università di Tor Vergata, Via della Ricerca Scientifica, 1-00133 Rome, Italy*

^d *Istituto Nazionale di Fisica Nucleare—Laboratori Nazionali del Gran Sasso, S.S. 17 BIS km. 18.910-67010 Assergi, Italy*

Received 27 April 2005; received in revised form 25 May 2005; accepted 26 May 2005

Available online 29 June 2005

Abstract

The results on cosmic rays detected by the gravitational antenna NAUTILUS have motivated an experiment (RAP) based on a suspended cylindrical bar, which is made of the same aluminum alloy as NAUTILUS and is exposed to a high energy electron beam. Mechanical vibrations originate from the local thermal expansion caused by warming up due to the energy lost by particles crossing the material. The aim of the experiment is to measure the amplitude of the fundamental longitudinal vibration at different temperatures. We report on the results obtained down to a temperature of about 4 K, which agree at the level of $\sim 10\%$ with the predictions of the model describing the underlying physical process.

© 2005 Elsevier B.V. All rights reserved.

PACS: 04.80.Nn; 95.55.Ym; 41.75.Fr; 96.40.–z; 61.82.Bg

Keywords: Gravitational wave detectors; Cosmic rays; Radiation acoustics

* Corresponding author. Tel.: +39 6 94032799; fax: +39 6 94032900.

E-mail address: alessandro.marini@inf.infn.it (A. Marini).

¹ Also at Dipartimento di Ingegneria Strutturale e Geotecnica, Università La Sapienza, Rome, Italy.

² Now at Istituto Nazionale di Fisica Nucleare—Sezione Roma1, Rome, Italy.

1. Introduction

Cosmic rays generate signals in a massive gravitational wave (GW) detector. The signals are due to vibrations produced by the heating along the particle trajectories, depending on the thermal expansion coefficient and on the specific heat of the material.

For cylindrical detectors the acoustic model [1–9] gives quantitative predictions for the amplitude of the longitudinal modes of oscillation due to the energy loss of a particle impinging on the cylinder. The amplitude is proportional to the ratio of the thermal expansion coefficient to the heat capacity. This ratio is part of the definition of the material Grüneisen parameter:

$$\gamma = \frac{\beta K_T V_m}{c_v}$$

where β is the volume expansion coefficient, K_T is the bulk module at constant temperature, V_m is the molar volume and c_v is the specific heat at constant volume. The parameter γ is nearly constant over a wide range of temperatures.

Cosmic ray measurements made with the aluminum GW detector NAUTILUS gave essentially two types of results:

- When the NAUTILUS bar was at a temperature $T = 0.14$ K, that is in a superconductive regime, the rate of the high energy signals due to cosmic ray showers was larger by two–four order of magnitude than the expectations based on the models [10,11].
- When the bar temperature was $T = 1.5$ K, aluminum in a normal state, few signals were large, most of the signals obeying [12] the predictions.

It was not clear to us whether that depended on the behavior of the Grüneisen parameter in the superconductive regime (for example, data on the aluminum critical field as a function of pressure and temperature [13] suggest absolute values of the parameter larger than in the normal state [14]).

To gain information on this problem a new experiment (RAP) was designed, consisting in bombarding a small aluminum bar, whose temperature we could control, with a known electron

beam, provided by the Beam Test Facility (BTF) of the DAΦNE Φ -factory complex at the INFN Laboratory in Frascati.

We compare the measured maximum amplitude of the bar fundamental longitudinal mode of oscillation with the expected value:

$$B_{th} = B_0(1 + \epsilon) \quad (1)$$

where [3]

$$B_0 = \frac{2}{\pi} \frac{\alpha L}{c_v M} W \quad (2)$$

Here, α is the linear thermal expansion coefficient ($\beta = 3\alpha$ for aluminum), L , M are respectively length, mass of the cylinder and W is the total energy released by the beam to the bar. The term ϵ accounts for corrections estimated by Monte Carlo methods due to contributions $O[(R/L)^2]$, R being the cylinder radius, and to the beam structure (see Appendix A).

A dilution refrigerator is needed to operate the bar in the superconductive regime. On the other hand, the assessment of the acoustic models down to low temperatures is in the range of interest of those GW aluminum resonant detectors that are now operated in the normal state of conduction. For this reason we decided to perform a first phase of the experiment covering the temperature interval 4–270 K, also with the purpose of testing the experimental setup and procedures to be employed later below 1 K, the second phase of the experiment including the dilution refrigerator.

After a short description of the experimental setup and a discussion on the beam simulated interactions within the bar, we report on the results obtained down to a temperature of ~ 4 K.

2. Experimental setup

The RAP setup is composed by the beam [15] and the detector [16,17]. The cylindrical test mass, the suspension system, the cryogenic system, the transducer and the data acquisition system are parts of the detector.

2.1. Beam

DAΦNE BTF provides the controlled beam for RAP. Although the facility is optimized for the

production of single electrons (or positrons), mainly for high energy detector calibration and testing purposes, it can provide particles in a wide range of energy (25–750 MeV) and intensity (up to $\sim 10^{10}$ particles/pulse). Particles can be produced in pulses of 1 or 10 ns duration, with a fairly uniform distribution. The maximum energy of the beam is ~ 510 MeV when BTF is jointly operated with the injections into the DAΦNE collider. The installation site of RAP is 2.5 m far away from the exit of the beam (see Fig. 1). The position of the beam at the exit of the line and at the entrance of the cryostat was monitored shot-by-shot by two high sensitivity fluorescence flags, 1 mm thick alumina doped with chromium targets. The spot size at the entrance of the cryostat, 50 cm far from the center of the bar, is ~ 2 cm in diameter. The

Monte Carlo simulation of the detector (see Section 4) indicates that the beam spot at the surface of the cylindrical bar maintains almost this dimension, due to negligible effects induced by the thickness of the cryostat vacuum shields intercepted by the beam.

BTF delivers to RAP single pulses containing $O[10^8]$ electrons each. In this range standard beam diagnostics devices to monitor the beam charge have low sensitivity, while saturation affects particle detectors. Therefore a monitor (BCM), based on an integrating current transformer readout by a charge digitizer, was installed to measure the pulse charge. The device accuracy is $\sim 3\%$ and the sensitivity, dominated by the digitizer, is $\sim 1.4 \times 10^7$ electrons, corresponding to a $\sigma \sim 4 \times 10^6$ electrons. The device is equipped with a calibration coil used to control the gain, the noise and the time shaping of the generated signals.

2.2. Test mass and suspension system

The oscillating test mass is a cylindrical bar (diameter 0.182 m, length 0.5 m, and mass 34.1 kg) made of Al5056, the same aluminum alloy (5.2% Mg, 0.1% Mn, and 0.1% C) used for NAUTILUS. The resonance frequency of the first longitudinal mode of vibration is 5096 Hz at $T = 296$ K.

The suspension is an axial-symmetric system of seven attenuation stages in series made of copper. The system provides a -150 dB attenuation of the external mechanical noise in a frequency window spanning from 1700 to 6000 Hz. The symmetry axis of the suspension passes through the center of mass of the cylinder. The suspension is linked to the lateral surface of the cylinder by means of two brass screws at the mid-section of the cylinder.

2.3. Cryogenic system

The cryogenic system is based on a commercial cylindrical cryostat (3.2 m height and 1.016 m diameter) and a $^3\text{He}^4\text{He}$ dilution refrigerator (base temperature = 100 mK, cooling power at 120 mK = 1 mW), to be installed in the near future. Cryogenic operations start by the filling of the cryostat with liquid nitrogen, both in the nitrogen

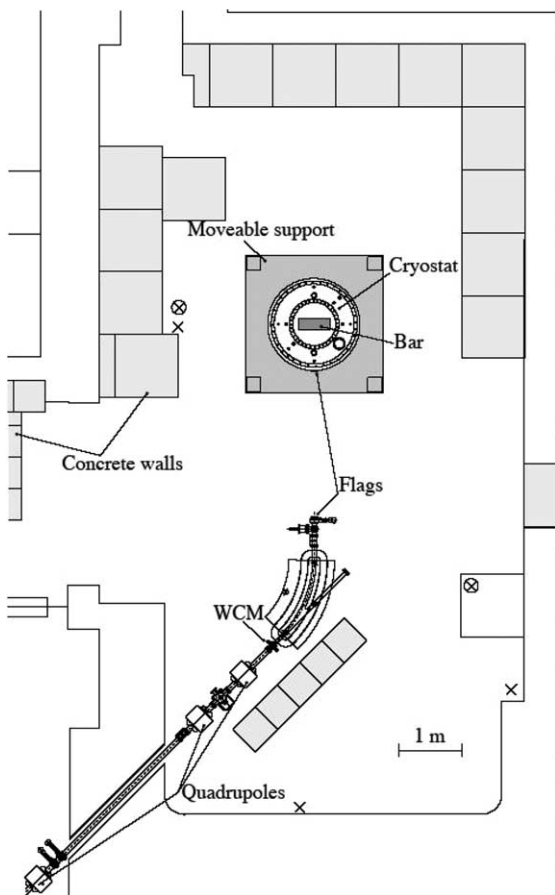


Fig. 1. Schematic layout of the RAP setup in the BTF hall.

and in the helium dewars, followed by the cool-down to 4.2 K with liquid helium. The thermal exchange among liquid helium and the bar is realized by filling the space surrounding the bar with ~ 1 mbar of gaseous helium. This is indeed the only thermal link between the bar and the liquid helium, the suspension-bar assembly being mechanically disconnected from the cryostat, with the exception of three thin stainless steel wires connecting the two components.

Temperatures are measured by two platinum resistor and three ruthenium dioxide resistor thermometers, in the 60–300 K range and in the 0–60 K range respectively, with a precision of 0.1 K. All the thermometers are controlled by a multi-channel resistance bridge.

A mechanical structure encloses the cryostat allowing an easy positioning of the detector on the beam line and the consequent removal after the expiration of the dedicated periods of data taking.

Fig. 2 shows the bar suspended inside the upper half of the cryostat.

2.4. Transducer and data acquisition system

Two Pz24 piezoelectric ceramics ($0.01 \times 0.01 \times 0.005$ m³), electrically connected in parallel, are



Fig. 2. The suspended bar in the opened cryostat.

inserted in a slot cut in the position opposite to the bar suspension point and are squeezed when the bar contracts. In this configuration the stress measured at the bar center is related to the displacement of the bar faces. The generated voltage signal is sent to an amplifier ($V_{\text{noise}} \sim 4$ nV/ $\sqrt{\text{Hz}}$). The data acquisition system (DAQ), based on a peak sensing 16-bit VME ADC and a VME Pentium III CPU running Linux, collects and stores on disk amplified data coming from the transducer and data originated from the thermometers and from the beam monitoring system. The acquisition system provides also tools for performing a fast inline analysis of the collected data.

3. Calibrations

It is possible to measure the value of λ , the transducer electro-mechanical coupling factor, making use of the electric equivalent circuit shown in Fig. 3.

This circuit includes a R_1 – L_1 – C_1 series that expresses the bar characteristics (dissipation, mass, and elasticity) and in parallel the Pz24's with capacity C_2 . To measure the equivalent circuit parameters, we proceed as follows:

- We apply a signal $V_g \cos(\omega_0 t)$ at the Pz24's for a time Δt much smaller than the decay time of the oscillations, where $\omega_0 = 2\pi f_0 = 1/\sqrt{L_1 C_1}$ is the angular resonance frequency of the bar.
- We switch the Pz24's from the oscillator producing V_g to the amplifier and measure the signal $V_0 \cos(\omega_0 t + \phi)$ due to the bar oscillation.

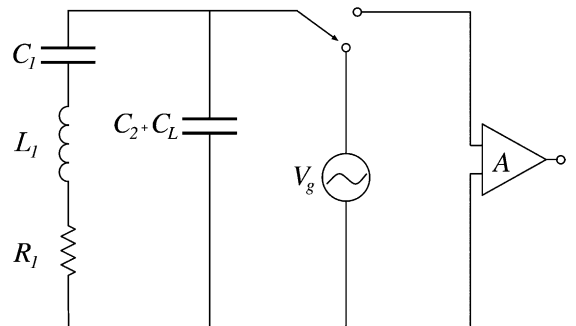


Fig. 3. Equivalent electrical circuit and calibration scheme.

Table 1

Frequency, decay time of the first mode of longitudinal oscillation and transducer coupling factor as a function of temperature

T [K]	f_0 [Hz]	τ_0 [s]	λ [10^7 V/m]
264	5143.7	6.25	1.32
71	5397.3	24	1.48
4.5	5412.7	84	1.32

It is possible to show [18] that C_1 is given by the following equation:

$$C_1 = \frac{V_0}{V_g \Delta t \pi f_0} [C_2 + C_L]$$

where C_L is the load capacity that includes the cable and the input impedance of the amplifier. Having measured the value of C_1 , we obtain λ for the first mode of longitudinal oscillation by

$$\lambda = \frac{2\pi f_0}{C_2 + C_L} \sqrt{\frac{MC_1}{2}} \quad (3)$$

where M is the mass of the bar.

The values of λ , obtained at different temperatures and before the collection of data useful for the estimation of the vibrational effects induced by the beam, are shown in Table 1 together with the measured frequency of the first mode of longitudinal oscillation f_0 and the its decay time τ_0 .

The Pz24's are inserted at a distance of ~ 0.09 m from the cylinder axis, while the calibration procedure we have used is correct in the $(R/L)^2 \ll 1$ approximation. We checked the calibration procedure inserting a commercial calibrated accelerometer with 5% accuracy at the center of one of the bar end surfaces. At room temperature the displacement measured by the Pz24's was 2.4% smaller than the one measured by the accelerometer and at $T \sim 77$ K the displacement was $\sim 6\%$ smaller. Consequently we assume a 6% systematic error in measuring the displacement amplitudes.

4. Simulation of the beam energy loss in the aluminum bar

We have developed a Monte Carlo simulation using the CERN package GEANT 3.21, taking

into account the real geometry and material of the cryostat and of the bar, and a realistic parametrization of the BTF beam, i.e., the beam spot size and divergence, and simulating the passage of electrons through the matter. The size of the beam spot and its angular and momentum spread have been simulated according to the measured characteristics: the well focussed BTF beam has a fairly Gaussian shape in the transverse plane with $\sigma_x = \sigma_y = 0.005$ m, the momentum spread is $\sim 1\%$ and the beam emittance is $\epsilon = 1$ mm mrad. The cryostat has been schematized as a succession of three coaxial aluminum cylinders. Due to the presence of these aluminum shields, with a total Al depth of 1.7×10^{-2} m, the energy of the electrons is slightly degraded by the emission of Bremsstrahlung photons. On average, more than 100 secondary particles are produced for each 510 MeV primary electron entering the bar. The spatial distribution of these secondary particles inside the bar is shown in Fig. 4 for the three perpendicular projections. The development of the electromagnetic shower is clearly visible; indeed the bar diameter corresponds to ~ 2 radiation lengths.

The total energy released to the bar by an electron in the beam is then evaluated adding the contribution of the energy lost by all the N_i secondary particles ($j = 0$ is the contribution of the primary electron itself), at each of the M_j tracking steps in the simulation code:

$$\Delta E = \sum_{j=0}^{N_i} \sum_{k=1}^{M_j} \Delta E_{jk}$$

The distribution of the energy lost by one electron with energy of 510 MeV in 10^6 trials, as shown in Fig. 5, leads to an average energy loss per electron:

$$\langle \Delta E \rangle \pm \sigma_{\Delta E} = 195.2 \pm 70.6 \text{ MeV} \quad (4)$$

and for a beam composed by N electrons to a total energy loss:

$$W = N \langle \Delta E \rangle, \quad \sigma_W = \sqrt{N} \sigma_{\Delta E} \quad (5)$$

We performed extensive simulations (see Appendix A) in order to: (a) apply the acoustic model to each infinitesimal step of the tracked particles, (b) include the treatment of the longitudinal

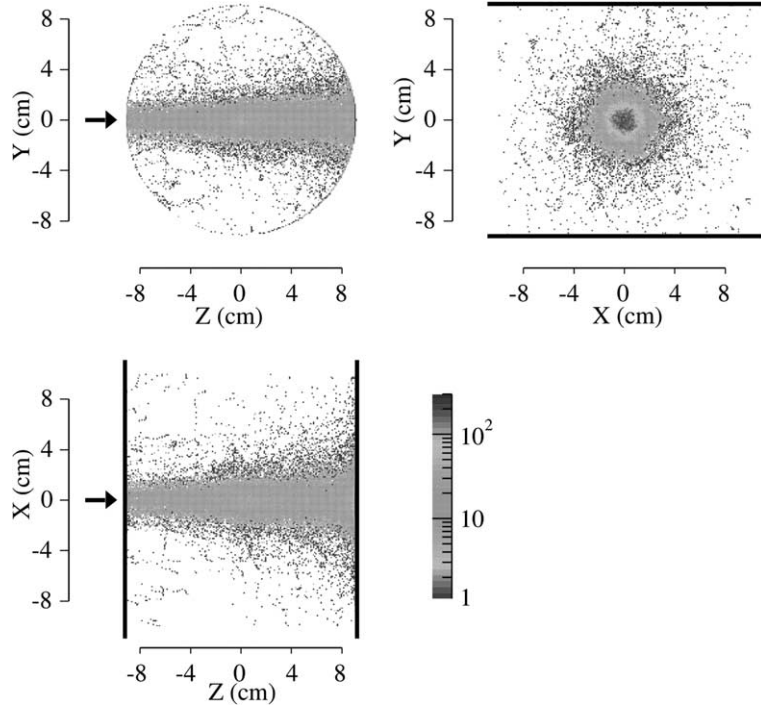


Fig. 4. Monte Carlo simulation: secondary particles distribution for 510 MeV primary electrons impinging on the bar for the three projections. The black arrow indicates the direction of the incoming beam.

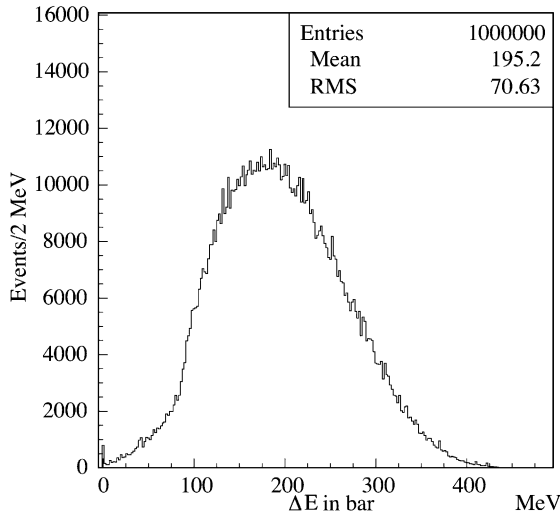


Fig. 5. Monte Carlo simulation for 510 MeV primary electrons impinging on the bar: ΔE per electron.

modes of oscillation at $O[(R/L)^2]$, (c) evaluate the effects due to the beam structure. This study leads to a value of -0.04 for ϵ in Eq. (1).

5. Measurements and comparison with expectations

Several electron pulses were applied to the bar at various temperatures (264 K, 71 K, and 4.5 K) with DAQ collecting ADC data, thermometer data and number of electrons per pulse. The maximum amplitude of the first longitudinal mode of oscillation of the bar, B_m , is related to experimental measured values according to the relation

$$B_m = V_{\max}/(G\lambda)$$

where V_{\max} is the maximum amplitude of the component of the signal at the frequency corre-

Table 2

B_0 due to $W = 10^{-3}$ J and input values for the calculation in case of pure aluminum

T [K]	α [10^{-6} K^{-1}]	c_v [$\text{J mol}^{-1} \text{ K}^{-1}$]	B_0 [10^{-13} m]
264	22.2	23.5	2.32
71	7.5	7.94	2.32
4.5	5.8×10^{-3}	7.6×10^{-3}	1.88

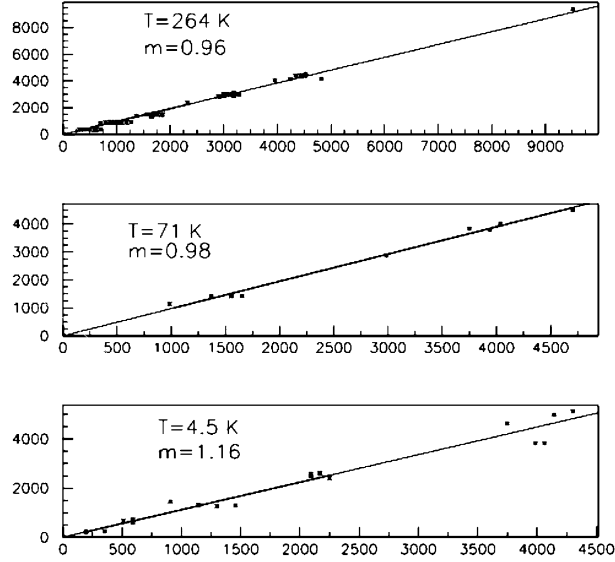


Fig. 6. Measured maximum amplitudes [10^{-16} m] of induced vibrations, B_m (vertical), versus the expected ones, B_{th} (horizontal), for various beam intensities. Straight lines are the least square fits with equation $B_m = m B_{th}$.

sponding to the first longitudinal mode, obtained using Fast Fourier Transform procedures applied to the ADC stored data, G is the gain of the amplifier and λ is the coupling factor defined in Eq. (3).

Knowledge of $\alpha(T)$ and $c_v(T)$ for aluminum is needed for computing the relation (2) at different temperatures: spline interpolations on data of Ref. [19] ($12 \text{ K} < T \leq 300 \text{ K}$) and the parametrization in Ref. [20] ($T \leq 12 \text{ K}$) give $\alpha(T)$, while $c_v(T)$ is obtained by spline interpolations on values of c_p reported in Ref. [21]. Table 2 shows the calculated values of α , c_v , B_0 due to a deposition of 10^{-3} J in a RAP-like bar made of pure aluminum.

The correlations among measured B_m and estimated B_{th} (Eq. (1)) are shown in Fig. 6 and the values of the parameter m fitting the relation $B_m = m B_{th}$ are shown in Table 3. A systematic er-

ror of $\sim 7\%$, obtained from the quadrature of the beam monitor (3%) and λ determination (6%) accuracies, affects the measurements.

6. Conclusions

The results we obtained for the maximum amplitude of the fundamental mode of longitudinal vibration of the bar are in good agreement with the expectations coming from the thermo-acoustic model describing the particle energy loss conversion into mechanical energy in the temperature range 270–4 K. This is the first time that experimental results on thermo-acoustic energy conversion in Al5056 are obtained below 270 K using our technique. The result at $T \sim 270 \text{ K}$ improves the agreement with the model when compared to the findings of past experiments [3,22] based on the same technique. Amplitude measured values at $T \sim 4 \text{ K}$ are slightly higher than expectations: this is probably due to a different behavior of Al5056 respect to pure aluminum or to an imperfect knowledge of the input parameters for the calculations in a region of temperatures where the ratio α/c_v sensibly depends on T .

Table 3
Values of m fitting $B_m = m B_{th}$

T [K]	m	Δm
264	0.96	0.01
71	0.98	0.03
4.5	1.16	0.03

Acknowledgements

We are greatly indebted to Dr. S. Bertolucci for the continuous support given to the experiment, to Drs. D. Babusci and G. Giordano for having derived the formal expression of the divergences used in the simulations of Appendix A and to Prof. M. Bassan for many useful discussions. We would like to thank Messrs. G. Ceccarelli, R. Ceccarelli, M. De Giorgi for the help given during the cryogenic operations of the detector and Messrs. M. Iannarelli and R. Lenci who helped with the experiment readout setup. This work is partially supported by the EU project ILIAS (RII3-CT-2004-506222).

Appendix A. Monte Carlo simulation

The energy in the normal modes of order n of a thin cylindrical bar (radius R much smaller than the length L) of mass M excited by a ionizing particle, can be calculated using the thermo-acoustic model [9] in terms of the sound source Σ , of the thermo-mechanical parameters of the bar and a geometrical factor G_n :

$$\begin{aligned} E_n &= \frac{1}{2M} \left(\frac{L \cdot G_n}{v_s} \cdot \Sigma \right)^2 \\ &= \frac{1}{2M} \left(\frac{L \cdot G_n}{v_s} \cdot \gamma \frac{dE}{dx} \right)^2 \end{aligned} \quad (\text{A.1})$$

where γ is the Grüneisen parameter, v_s is the speed of sound, dE/dx is the specific energy loss. The geometrical factor G_n , taking into account the path A inside the bar and the coupling to the eigenmodes of frequency ω_n , is defined as the path integral of the divergence of the displacement vector (normalized to the volume) \vec{u}_n :

$$G_n = \frac{v_s}{\omega_n} \frac{1}{A} \int_A \left(\vec{\nabla} \cdot \vec{u}_n \right) dl \quad (\text{A.2})$$

In other terms, the energy for the n th mode is obtained by squaring the amplitude of the vibration for a path of a single ionizing particle inside the bar:

$$E_n = \frac{1}{2M} \frac{\gamma^2}{\omega_n^2} \cdot A_n^2$$

The corresponding expression when the bar is crossed by N particles is given by summing (incoherently) over all the amplitudes,

$$A_n = \sum_{i=1}^N A_n^{(i)}$$

so that Eq. (A.1) can be written as

$$E_n = \frac{1}{2M} \frac{\gamma^2}{\omega_n^2} \left(\sum_{i=1}^N A_n^{(i)} \right)^2 \quad (\text{A.3})$$

In the estimate of the expected amplitude when a beam of particles crosses the bar, two extreme approaches are possible: the specific energy loss is assumed to be constant all along the trajectory inside the resonant bar, so that it can be computed separately from G_n ; or the real energy loss is evaluated for each infinitesimal step and is multiplied by the correct geometrical factor before summing all the amplitudes:

$$A_n = \sum_{i=1}^N \int_{A_i} \left(\vec{\nabla} \cdot \vec{u}_n \right) \frac{dE}{dl_i} dl$$

The latter method requires a simulation of the elementary processes of energy loss inside the material. The GEANT routines are able to track all the secondary particles produced in the interaction with the material of the generated (primary) particle, and all the different physical processes occurring when the particles cross the matter are simulated, taking into account the appropriate cross-sections for the different materials in the set-up, and the current energy and momentum of the particle: ionization, Coulomb scattering, and Bremsstrahlung for charged particles; pair production, Compton scattering, and photoelectric effect for photons.

All the secondary particles produced in the interactions with the matter are followed until their energy falls below a given threshold. The size of the step of the simulation for each particle is automatically adjusted, in order to optimize the accuracy vs. the computing time, taking into account the set-up geometry and materials together with the kinematical quantities of the currently tracked particle.

Such a simulation code is well suited to include the calculation of the geometrical integral in the tracking routines, together with the evaluation of the specific energy loss for the different physical processes happening inside the materials, at each step of the simulation. Moreover, since the contribution of each single particle in the beam has to be added in an incoherent sum, it is easy to extend the sum over all the secondary particles of the electromagnetic shower that develops inside the bar for each incident electron.

The total excitation amplitude for the i th primary electron in the beam is then evaluated adding the contribution of all the N_i secondary particles ($j = 0$ is the contribution of the primary electron itself), at each of the M_j tracking steps in the simulation code:

$$A_n^{(i)} = \sum_{j=0}^{N_i} \sum_{k=1}^{M_j} a_n^{(jk)}$$

By summing together the contribution of all the steps of all the tracked particles, quantities such as the total path length:

$$\Delta x = \sum_{j=0}^{N_i} \sum_{k=1}^{M_j} \Delta \vec{x}_{jk}$$

and the total energy loss:

$$\Delta E = \sum_{j=0}^{N_i} \sum_{k=1}^{M_j} \Delta E_{jk}$$

can be calculated for each incoming primary electron.

The integral in the expression of G_n is numerically calculated for each step, assuming that the divergence of the displacement vector is constant (this is a good approximation for steps of ~ 1 mm):

$$\begin{aligned} a_n^{(jk)} &= \int_{A_j} (\vec{\nabla} \cdot \vec{u}_n) \frac{dE}{dl_j} dl_j \\ &= \sum_{k=1}^{M_j} (\vec{\nabla} \cdot \vec{u}_n(\vec{x}_{jk})) \cdot \Delta E_{jk} \end{aligned} \quad (\text{A.4})$$

In order to compute the divergence $\vec{\nabla} \cdot \vec{u}_n(\vec{x}_{jk})$, the exact solution of the normal modes of a finite cylindrical bar have been replaced by the approximate solution for an infinite cylinder due to

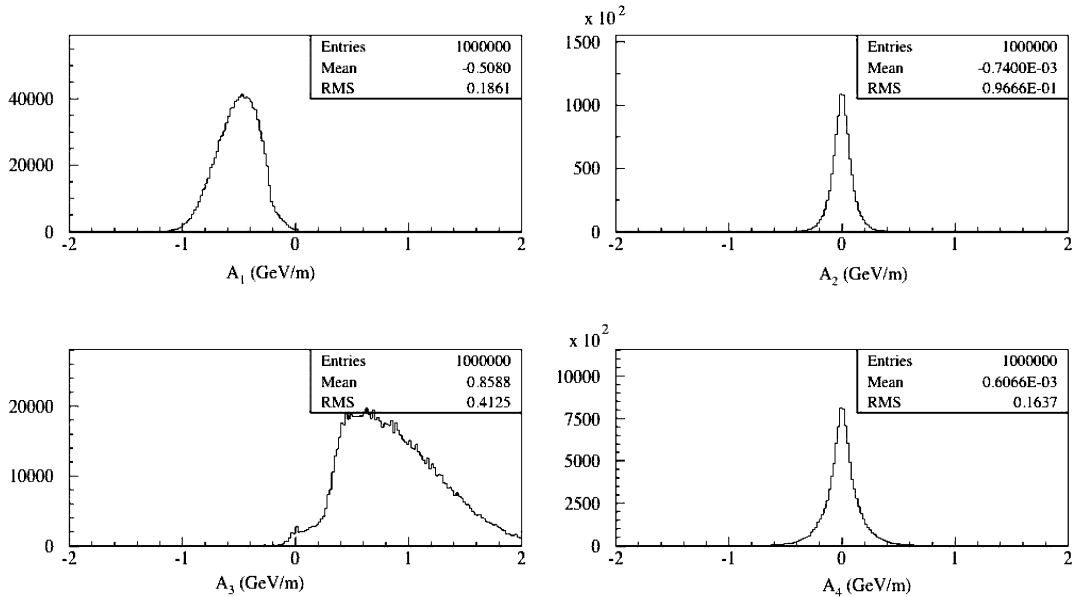


Fig. A.1. Monte Carlo results for the first four modes of the amplitude: on the left the odd modes ($n = 1, 3$), on the right the even modes ($n = 2, 4$) distributions (on top, bottom respectively). In the histograms all the events from 100 simulated shots of 10^4 electrons with $E = 510$ MeV have been accumulated.

Pochhammer and Chree (PC). This approximation holds for a thin cylinder, i.e., as long as $\alpha_n = n\pi \frac{R}{L} < 1$. The PC solution has been expanded to the order $O[\alpha_n^2]$ leading to:

$$\vec{\nabla} \cdot \vec{u}_n(\vec{x}_{jk}) = \frac{\sqrt{2}\alpha_n}{R} \left[1 + \frac{\sigma(1-\sigma)}{4} \alpha_n^2 \right] \times \left[2\sigma - 1 + \frac{\sigma}{2} \left(\alpha_n \frac{r}{R} \right)^2 \right] \sin \left(\alpha_n \frac{z}{R} \right)$$

where σ ($= 0.347$ for isotropic aluminum at room temperature) is the Poisson module and r, z are referred to a cylindrical coordinate system having the z -axis coincident with the bar axis and the z -origin located at one of the bar end surfaces.

In order to simulate a number of beam pulses on the RAP bar, the vibrational amplitudes in the different normal modes have been computed simulating a given number of electrons in the beam, with the nominal energy of 510 MeV and with the proper beam spread and divergence. This gives an estimate of the bar response for a given beam intensity. The following results refer to 100 pulses of 10^4 electrons/pulse, hitting the bar at the center.

The distributions of the A_n amplitudes for the first four modes are shown in Fig. A.1. The odd modes have a non-zero average, while the average for the even modes is consistent with zero. This is what we expect from the properties of the eigen-functions, that are symmetric (anti-symmetric) with respect to $z = L/2$ for odd (even) modes. Since the beam enters the bar at $z = L/2$, $A_{n=1,3,\dots}$ will have the same sign; while $A_{n=2,4,\dots}$ will change sign and have a null expectation value.

In order to obtain an estimate of ϵ (Eq. (1)) from this full simulation we compare the average value of $A_1 = -0.508$ GeV/m, derived from the

corresponding histogram of Fig. A.1, against the value of A_1 when computed $O[\alpha^1]$:

$$A_1 = \frac{\sqrt{2}\pi}{L} (2\sigma - 1) \langle \Delta E \rangle = -0.530 \text{ GeV/m}$$

which is related to Eq. (2) in the hypothesis that all the energy lost by an electron (cf. Eq. (4)) is deposited at the bar center. Thus we obtain $\epsilon \sim -0.04$.

References

- [1] B.L. Beron, R. Hofstadter, Phys. Rev. Lett. 23 (1969) 184.
- [2] B.L. Beron et al., IEEE Trans. Nucl. Sci. 17 (N1) (1970) 65.
- [3] A.M. Grassi Strini, G. Strini, G. Tagliaferri, J. Appl. Phys. 51 (1980) 948.
- [4] A.M. Allega, N. Cabibbo, Lett. Nuovo Cim. 38 (1983) 263.
- [5] V.A. Malugin, A.B. Manukin, in: L.M. Lyamshev (Ed.), Radiation Acoustics, CRC Press, 2004, p. 301.
- [6] C. Bernard, A. De Rujula, B. Lautrup, Nucl. Phys. B 242 (1984) 93.
- [7] A. De Rujula, S.L. Glashow, Nature 312 (1984) 734.
- [8] E. Amaldi, G. Pizzella, Nuovo Cim. C 9 (1986) 612.
- [9] G. Liu, B. Barish, Phys. Rev. Lett. 61 (1988) 271.
- [10] P. Astone et al., Phys. Rev. Lett. 84 (2000) 14.
- [11] P. Astone et al., Phys. Lett. B 499 (2001) 16.
- [12] P. Astone et al., Phys. Lett. B 540 (2002) 179.
- [13] E.F. Harris, D.E. Mapother, Phys. Rev. 165 (1968) 522.
- [14] A. Marini, J. Low Temp. Phys. 133 (2003) 313.
- [15] G. Mazzitelli et al., Nucl. Instr. Meth. A 515 (2003) 524.
- [16] S. Bertolucci et al., Classical Quant. Grav. 21 (2004) S1197.
- [17] P. Valente et al., Nucl. Instr. Meth. A 518 (2004) 261.
- [18] G.V. Pallottino, G. Pizzella, Nuovo Cim. B 45 (1978) 275.
- [19] F.R. Kroeger, C.A. Swenson, J. Appl. Phys. 48 (1977) 853.
- [20] J.G. Collins, G.K. White, C.A. Swenson, J. Low Temp. Phys. 10 (1972) 69.
- [21] CRC Handbook of Chemistry and Physics, 73rd ed., CRC Press, 1992.
- [22] G.D. van Albada et al., Rev. Sci. Instr. 71 (2000) 1345.